EUR 4743 e

DEEP PENETRATION OF NEUTRONS IN HYDROGENOUS SHIELDS

by

B. CHINAGLIA and G. BOSIO
(SORIN)

(Topical Report)

1972

LEGAL NOTICE

This document was prepared under the sponsorship of the Commission of the European Communities.

Neither the Commission of the European Communities, its contractors nor any person acting on their behalf ;

make any warranty or representation, express or implied, with respect to the accuracy, completeness, or usefulness of the information contained in this document, or that the use of any information, apparatus, method or process disclosed in this document may not infringe privately owned rights; or

assume any liability with respect to the use of, or for damages resulting from the use of any information, apparatus, method or process disclosed in this document.

This report is on sale at the adresses listed on cover page 4

at the price of B.Fr. 50.—

EUR 4743 e

The penetration of fission neutrons in hydrogenous shields has been measured by means of activation detectors in well defined geometrical conditions.
The experimental results refer to:
a) Al-27 (n, α) reaction rate in water, measured up to 2.1 m from the Avogadro RS1 reactor core;
b) several detector reaction rates covering the energy range from thermal to the Al-27 (n, α) threshold in an iron-water lamination up to 1.5 m from a disk source (EURACOS facility of CCR Euratom Ispra).

The investigated thicknesses are greater than those previously reported in the literature for similar media and calculation errors which might be relevant for reactor shield design can be detected by comparison with the present experiment. The experimental results are therefore given in full detail together with the source description to permit their use for meaningful tests of shielding codes.

As examples of such tests the following results have been obtained for the shielding codes QAD and SABINE:
— the Moment Method data for water above ∼ 6 MeV calculated up to 1.6 m (water density 1 g/cm^2) reported in ORNL 3487 are confirmed within 10 %; exponential extrapolation of the attenuation kernel beyond this distance yields a slight under-estimate of the flux at 2.1 m. When the neutron dose is considered it is expected that the QAD predictions obtained using the exponential fitting of the above data are somewhat lower than the true values at this distance, but the discrepancy should not exceed a factor 2;
— the SABINE thermal flux is in excellent agreement with the experimental data in the iron-water mixture. Fast fluxes are somewhat underestimated beyond 1 m in iron-water and, to a greater extent, in plain water. This effect seems to derive from the removal cross sections of water and a small decrease in their values yelds reasonable agreement with the experimental data.

EUR 4743 e

DEEP PENETRATION OF NEUTRONS IN HYDROGENOUS SHIELDS

by

B. CHINAGLIA and G. BOSIO

(SORIN)

(Topical Report)

1972

ABSTRACT

The penetration of fission neutrons in hydrogenous shields has been measured by means of activation detectors in well defined geometrical conditions.

The experimental results refer to:

a) Al-27 (n, α) reaction rate in water, measured up to 2.1 m from the Avogadro RS1 reactor core;

b) several detector reaction rates covering the energy range from thermal to the Al-27 (n, α) threshold in an iron-water lamination up to 1.5 m from a disk source (EURACOS facility of CCR Euratom Ispra).

The investigated thicknesses are greater than those previously reported in the literature for similar media and calculation errors which might be relevant for reactor shield design can be detected by comparison with the present experiment. The experimental results are therefore given in full detail together with the source description to permit their use for meaningful tests of shielding codes.

As examples of such tests the following results have been obtained for the shielding codes QAD and SABINE:

— the Moment Method data for water above ~ 6 MeV calculated up to 1.6 m (water density 1 g/cm^3) reported in ORNL 3487 are confirmed within 10 % ; exponential extrapolation of the attenuation kernel beyond this distance yields a slight under-estimate of the flux at 2.1 m. When the neutron dose is considered it is expected that the QAD predictions obtained using the exponential fitting of the above data are somewhat lower than the true values at this distance, but the discrepancy should not exceed a factor 2;

— the SABINE thermal flux is in excellent agreement with the experimental data in the iron-water mixture. Fast fluxes are somewhat underestimated beyond 1 m in iron-water and, to a greater extent, in plain water. This effect seems to derive from the removal cross sections of water and a small decrease in their values yelds reasonable agreement with the experimental data.

KEYWORDS

Index *)

---

1. Introduction

It is well known that rather large errors may affect the prediction of the neutron flux far from the source (more than ~ 10 relaxation lengths). The failure of the diffusion theory for shield calculation is the major example evidenced since long time, but even more exact solutions are based on, or imply, assumptions and approximations which may be uncorrect at deep penetration (for instance the number of angular interval divisions in a S_N code).

In any case, whatever computational method is used, the answer is dependent on the accuracy of basic data (cross section) and their average values within finite energy intervals. The error deriving from uncorrect cross section sets increases with the distance (for a pure exponential attenuation the relative error is proportional to the optical path) and can reach high values for real reactor shields.

The various effects due to the method, mesh intervals, cross sections are correlated and the basis for assessing the validity of a code is an experiment in known conditions.

This work has the scope to give some deep penetration results obtained during an experimental study of the neutron attenuation in water and iron-water mixtures. These media have been extensively investigated in the past with the main purpose to determine the detailed space-energy distribution in the first part of a shield and most of the published data* refer to penetration depths ranging from 50 to 100 cm.

---

* A survey of experimental results may be found in Ref.1.

Such depths however are well below the total thickness
of a shield. On the other hand in hydrogenous media the
absorption and energy degradation process is such that the
attenuation of the total flux is controlled by a fast neutron
component whose mean energy is increasing with the distance.

Therefore the flux behaviour at deep penetration could not
be extrapolated from the short distance data, where the most
energetic neutrons have a minor importance.

This work was originated for a particular problem and
some results which refer to the comparison between experiment
and calculation with the Shielding codes Sabine [7] and
QAD-P5 [8] are presented. The main emphasis is however given
to the experimental results and the source and shield characte
ristics are described in full detail to permit the use of the
data for other tests.

2. Experiments

2.1 - The plain water medium.

For the plain water medium the source is the core of the
Avogadro RS1 swimming pool reactor and the measurements have
been made on vertical and horizontal lines passing through
the center of the core.

The core consist of MTR type fuel elements having 19 pla-
tes (10 plates for control elements) of Al/U alloy 0,127 cm
thick separated by 0,287 cm of water as shown in fig.1. For
the source description the active zone of each element may be
considered a homogeneus mixture containing the following volu-

me ratios:

	Standard Element	Control Element (100% inserted)
V_{H_2O} / V_t	0,609	0,658
V_u / V_t	0,085	0,0479
V_{Al} / V_t	0,306	0,284

$$V_t \quad = \quad \text{total active volume of 1 element}$$
$$= \quad 3800 \text{ cm}^3$$

The power distribution is known from thermal flux measurements. Fig.2 shows the reactor loadings n.271 I and n.279 I which have been used for the present experiments; the numbers in each box representing an element are proportional to the thermal flux at the center of the element (between the two central plates at half the active length). The vertical profile is nearly identical for all the elements and a mean value is given in fig. 3a. The position of the control rods during the experiments is also shown in fig.2.

The neutron attenuation has been measured by the use of aluminium foils with the Al^{27} (n, α) reaction, along a vertical line passing through the water hole of the reactor loading n.271 I and a horizontal line for reactor loading n.279 I as shown in fig.2.

The choice of the detector has been dictated by several reasons:

- A high threshold detector is not sensitive to photoneutrons produced in water. The photoneutron flux is known to overcome the flux of fission born neutrons at low (thermal) energies beyond a distance of 2m in water, and the experimental results

would be of doubtful usefulness at this penetration in the case of low energy detectors.

- The low density of aluminum and the high γ energy of the reac tion product Na^{24} make possible the use of rather thick detectors without strong self-absorption during the activity counting. The detection limits can therefore be lowered by the use of large size detectors.

- The half period of 15 hours permits to reach easily activity values near to saturation and to make use of the decay after irradiation for lowering the very high counting rate ratio ($\sim 10^{12}$) between the most and less active detectors.

- The behaviour of high energy neutrons is particularly important and the Al^{27} (n, α) reaction may provide a direct test of the energetic component of the spectrum which controls the deep penetration of neutrons.

High purity (> 99,999) aluminum disks of various dimensions (diameter: 1,5 to 7 cm, thickness 0,1 to 0,2 cm) have been used as detectors. During irradiation they were wrapped in aluminum foil inside cadmium boxes to reduce surface contamination and activation of impurities from thermal neutrons. Furthermore after irradiation each detector was etched in NaOH solution to eliminate any surface contamination. The activity measurement has been performed with calibrated scintillation detectors (3"x3" NaI (Tl) crystals) at various source-detector distances using appropriate correction factors for the finite size of the disks. Further details of the experimental procedure are given in Ref.2.

The results are given in table I and also plotted in fig.4. The reactor power for the vertical axis, reactor loading n.271 I, was 5 Mw and for the horizontal axis, reactor loading n.279 I, 7 Mw.

In Ref. 2 and 3 an analysis of the errors has been made, and the following values have been obtained:

a) Counting statistics: only the less active detectors are affected by bad counting statistics. The standard deviation is given in table 1.

b) Reactor power: 10%.

c) Distance from the core: the position of the detectors with respect to the supporting frame is known with good precision, so that the distance between the various detectors has a negligible error; the position of the frame with respect to the source is defined with smaller precision. For the vertical axis measurements the uncertitude of the fuel length within the elements leads to an error of $\pm$ 1 cm, which corresponds to about 10% on the activity of detectors far from the source. For the horizontal axis some uncertitude arises from the curvature of fuel plates and the resulting error on the activity is $\pm$ 3%.

d) Perturbation due to the supporting frame: a negligible perturbation is evaluated.

e) Spurious contribution from activation of impurities (taking into account the contribution of photoneutrons to the low energy flux): less than 10^{-3} for the more distant detector.

f) Contribution to Al^{27} (n, α) reaction from photoneutrons: absent (an upper limit of $5 \cdot 10^{-4}$ is evaluated with largely conservative assumptions).

g) Absolute calibration of γ counter and correction factors: $\leqslant$ 5%

The resulting standard deviation is about 12% for horizontal and 15% for vertical axis measurements and it must be observed

that only the statical error (a), which is negligible up to about 1,5 m, affects the shape of the curve of fig.4.

2.2 - Iron - water lamination.

The source is the EURACOS facility of CCR-Euratom Ispra which is described in detail in Ref.4. Its essential features are:

- disk source, 0,8 m diameter, 90% enriched Uranium-235;
- well defined neutron spectrum;
- power: (1,25 $\pm$ 0,10) Kw.

The experimental shield configuration is an array of iron, water and air slabs as shown in fig.5. The iron slabs (transver sal dimensions 1,45 m x 1,45 m) are immersed in water inside an iron walled tank which during irradiation fills the void of the concrete tunnel of the EURACOS facility, as shown in the insert of fig.6.

Streaming along the unavoidable gap between tank and concrete walls was greatly reduced by the bends of the tank walls.
A streaming component was however detected as shown later and gave rise to a spurious contribution to the measurements at the end of the tank.

Starting from the source, the sequence of materials along the axis of fig.5 is given by the following table:

M	air	Fe	H_2O	Fe	H_2O	Fe	H_2O	Fe
t	26	1	11	3	3,5	8	10	10

M	air	Fe	H_2O	Fe	H_2O	Fe	H_2O	Fe
t	11,9	3,2	32,5	13	10	13	22,4	1

M : material

t : thickness of material M (in cm).

Reaction rates of various detectors were measured along
the axis of the shield by irradiating foils or pellets fixed
to lucite holders (in water) or to iron plugs (inside the iron
slabs). The reactions and the physical form of the detectors are
given below:

Dy^{164} (n, γ): Al/Dy alloy (10% or 30%); disks.

Au^{197} (n, γ): pure gold or Al/Au 0,1% alloy; disks.

In^{115} (n,n'): pure In; disks.

S^{32} (n, p): pure S; fused pellets.

Al^{27} (n, α): pure Al; disks.

All the above detectors, except Dy, were irradiated under
cadmium; the Cd thickness used for Au was 1 mm (cut-off at
~ 0,44 eV). Absolute saturation activities per gram element
were obtained by means of calibrated counters. Further details
on the experimental procedure are given in Ref.5.

The results are given in Table II and fig.7 as a function
of the distance z measured from the inner face of the tank wall,
expressed in reaction rates (R.R.) for In, S, Al detectors. For
Dy the data have been converted to thermal flux Φ_{th} (the con-
version is based on intercalibration of Dy and Au detectors in a
slowing down spectrum in water, using $\sigma_{Au} = 98$ b) and from Au/Cd
the epithermal flux per unit lethargy Φ_{u} has been calculated,
using a value 1550 b for the resonance integral.

In addition to the statistical error ϵ reported in Table 2,
the values are affected by uncertitude in the source power (8%),
position ($\pm$ 0,1 cm, which for fast neutron detectors is equiva-
lent to ~3%) and calibration of the counters ($\pm$ 5%).

Near the end of the tank the data have a spurious contribu-
tion due to neutron streaming along the gaps; fig.6 shows the

epithermal streaming flux measured around the tank. A correction has been made for this effect assuming that the streaming flux entering the end wall is attenuated exponentially in water with a relaxation length of 10 cm , as shown in fig.7. The corrected values are given in Table 2.

3. Calculation

Some calculation results obtained with QAD and Sabine are given in fig.s 4 and 7. Before discussing the comparison with the experimental data, it is useful to describe briefly the geometry and cross section sets used as inputs to the codes.

3.1 - Geometry.

The simple disk geometry of the Euracos source was descri bed exactly in both codes. The Avogadro reactor core source was approximated by one or more regions having power distributions obtained by averaging the values of fig.2 along the appropriate axis as described below.

Reactor loading n.271-I.

QAD: a single homogeneous source region was considered, bounded by planes:

x = 0	x = 50,7 cm
y = 0	y = 46,8 cm
z = 0	z = 68,4 cm

where z is a vertical axis and the origin is taken at the left lower corner of the core shown in fig.2.

In this rather coarse description the water hole C4 is considered a source element.

Sabine: no calculation has been made.

Reactor loading n.279-I.

The greater accuracy reached in the measurements along the horizontal axis suggested to use a more accurate description of the source for this case.

QAD: the core was divided in 3 regions:

1) rows 2, 3, 4, 5   power 5,344 Mw

2) "   6   "   0,929 Mw

3) "   7   "   0,727 Mw

The boundary planes are shown in fig.8b and the power distributions are given in fig.9.

Sabine: the core was divided in 2 cylindrical regions as shown in fig.8C. The power distribution along the z axis and the radial direction are given in fig.3a and 3b.

3.2 - Cross sections.

In QAD the attenuation kernel in water is fitted by $e^{- A_i d^i}$ where d is the water thickness. The coefficients A_i used for the present calculation for the various energy groups are given in Table III.

Three different removal cross section sets for water have been used for the Sabine calculation, they are shown in Table IV.

The activation cross section of the threshold detectors were derived from the best literature data.

The average values within the QAD groups are given in Table V and refer to a pure fission spectrum.

3.3 - Boundary conditions.

For the Sabine code the following boundary conditions have been used:

reactor: a value derived from in core measurements and a cal-

culated spectrum[9] has been assigned to every group flux

at the inner boundary. Transversal buckling:

$B^2 = 3,6 \cdot 10^{-3}$ cm^{-2} (from measurements).

Euracos: $J^+ = 0$ at the inner boundary for the first and the

thermal group, for the other groups calculation with $J^+ = 0$

and $J^+ > 0$ ($\Phi / \Phi' = (2+i)$ D for i 23; i = group index) gave

similar results except near the source. At the outer boundary:

zero incoming current.

4. Discussion and conclusion

The data reported in the previous sections have been

obtained in well defined conditions and can therefore be used

for meaningful tests of calculation methods. The investigated

thickness (2,1 m in water, 1,40 m effective thickness in iron

water) is sufficiently large to put in evidence errors which

might be relevant in reactor shield calculation. Some implica-

tions concerning the examined codes are given in the following.

4.1 - Water.

The comparison based on the Al (n, α) reaction in water

shows that the calculated data are somewhat lower than the

experimental ones at deep penetration.

4.1.1 - QAD.

The QAD results are examined firstly. Two geometry errors

affect the data at short distances:

- the first is the homogenization in reactor loading 271-I;
  a rough evaluation indicates that, if in reactor loading
  n.271-I the water hole is taken properly into account, the
  predictions near the core are to be lowered by about 30%;

- the second effect is characteristic of the integration

method, which for any volume element of the source appro-
ximates the mean value of the attenuation kernel with the
value calculated at the geometrical center of the element
itself. This error depends on the distance and on the size
of the volume elements and in the present case the flux
should not be overestimated by more than 5% at large di-
stance (above 1 m).

An error derives from the use of constant cross sections
based on a fission spectrum as used in the QAD groups. A cor-
rection factor may be calculated by weighing the cross sections
over the Moment Method spectrum[6]. This error is however of
little importance (below 10% in the range of distances inve-
stigated).

The values of the fitting coefficients A_i play a more
important role. When the fluxes given by these coefficients
are compared with the data of ref.6, it is found that the fit-
ting is rather poor at deep penetration; furthermore beyond
1,6 m no data are available and one must extrapolate the expo-
nential behaviour of the last fitted zone. This procedure is
certainly not conservative.

A correction factor has been calculated for taking into
account the two effects of cross section and uncorrect fitting.
This factor is the ratio of the Al(n, α) reaction rate calcula-
ted at various distances d in water from a point source with
the exact detailed shape of Ref.6 to that given by QAD for the
same conditions. As a results the QAD data of fig.4 should be
multiplied by:

0,85   for z   ~30 cm

1,10   "   70 cm

1,30   "   140 cm

where the hypothesis has been made that the correction factor

evaluated at a distance d from a point source applies to a distance $z = (d+20)$ cm for the core source.

The above corrections bring in excellent agreement experimental data and QAD predictions indicating that above 6 Mev the Moment Method results of Ref.6 are confirmed by the present experiments within 10%. The use of a constant cross section and of the fitting coefficients of Table III does not introduce large errors and even at about 2 m the ratio experimental over predicted reaction rate is lower than 2.

These findings indicate that at lower energies one should expect a better agreement or even conservative predictions, since the fluxes obtained with the coefficients Ai below 6 Mev are in much better agreement or overestimate those of the Moment Method.

4.1.2 - SABINE

A preliminary observation concerns the procedure followed to obtain the threshold detector reaction rates. Mean group activation cross sections are calculated for each group using the removal flux as weighing function. In the case of $Al^{27}(n, \alpha)$ reaction and water medium this procedure leads to a slight overestimate of the reaction rate since within the first group the total and removal flux spectra are quite different, the latter being strongly peaked at high energy.

This effect can be evaluated on the basis of the more realistic spectrum shape given by the Moment Method calculation[6].

Assuming that the spectrum at a distance z from the core has the same shape calculated at a distance z+ 20 cm from a point source, the Sabine predictions of fig. 4 should be lowered by:

$$8\% \quad at \quad z= 1 \ m$$
$$23\% \quad at \quad 1,6 \ m$$
$$28\% \quad at \quad 2,1 \ m$$

and therefore the discrepancies with the experimental points should be slightly increased.

The present comparison indicates that the removal cross section sets B and C of table IV are more adequate than set A for the description of the high energy neutron flux in water. This conclusion could be extrapolated to lower energy neutrons, since according to the calculation scheme the flux at any energy in water follows the removal flux attenuation far from the source.

4.2 - Iron - water lamination.

4.2.1.- QAD

As well known, when a shield is composed by one or more materials in addition to the reference material, use is made in the QAD code of an equivalent thickness

$$t'_M = t_M \ \Sigma_M / \Sigma_O$$

where:

t_M = thickness of material M

Σ_M = removal cross section of material M

Σ_O = removal cross section of the reference material.

In the present case the following values have been used:

Σ_O = 0,101 cm^{-1} (water)

Σ_M = 0,168 " (iron)

The comparison with experimental data has been limited to threshold detector reaction rates, calculated with activation group cross sections averaged over a fission spectrum.

An excellent agreement is found every where (see fig. 7) for high energy neutrons (above ~ 3 MeV, sulphur and aluminum data) and also for lower energy neutrons (above ~ 1 MeV, indium data) far from the iron slabs, as expected from the application of a removal cross section.

4.2.2.- Sabine

The calculation shown in fig. 7 has been made with the removal cross section set A of table IV.

The tendency to underestimate the fluxes is again observed, although the discrepancies with the experimental data are lower than in the previous experiment.

Threshold detector and epicadmium gold activation are somewhat underestimated whilst the thermal flux closely fits the experimental points (except at the interior of the iron slabs) over the whole shield.

A discussion of these findings is outside the scope of this work; it may be observed that a better agreement would be obtained by the use of the water removal cross sections B and C of table IV and that in a lamination where the water thickness is comparable to the iron thickness and does not exceed 30 cm the thermal diffusing flux never attains equilibrium with the removal flux and therefore in this range its attenuation does not depend strongly on the removal neutron attenuation.

Acknowledgments.

Part of this work has been performed at the Euratom CCR of Ispra and the authors wish to thank dr. Nicks, Perlini, and Ponti of the Euratom staff for assistance during the experiments and calculations.

REFERENCES

1) J.Butler and A.F. Avery in "Engineering Compendium on Radiation Shielding" ed. by R.G.Jaeger, Chapt.5 Springer Verlag - 1968.

2) G.Bosio, F.Magnani, F.Vallana "Confronto tra QAD-P5, SABINE e misure sperimentali in acqua per forti penetrazioni nel reattore Avogadro RS1 con rivelatore Al(n,α)". SORIN Report F/633 (1970).

3) B.Chinaglia, D.Monti "Confronto tra QAD e misure in acqua: reattore Avogadro" SORIN report F/599 (1969).

4) G. Perlini "Euracos: un dispositivo di irradiazione ad elevato flusso". En. Nucl. 15, 11 (1968).

5) B.Chinaglia, G.Bosio, F.Magnani, G.Del Zoppo "Esame sperimentale di uno schermo laminare ferro acqua a grandi distanze". SORIN report F/625 (1970).

6) D.K.Trubey - ORNL 3487 (1964).

7) C.Ponti, H.Preusch and H.Schubart "SABINE, a one dimensional bulk shielding program" Eur 3636 e (1967).

8) R.E.Malefant "QAD: a series of point kernel general purpose shielding programs" LA 3573 (1966).

9) M.Iman Atom Kernenergie 12-7 p.35 (1967).

FIGURES:

1_7 Fuel elements (standard and control) of Avogadro RS1 reactor.

2_7 Scheme of the reactor loadings used for the water esperiments. Numbers inside elements are proportional to the thermal flux values.

3_7 Vertical and radial power distribution (average values).

4_7 Attenuation of the Al^{27} (n, α) reaction rate in water.

5_7 Scheme of the experimental set-up used for iron-water experiments.

6_7 Neutron (fast and epithermal) streaming around the gap shown in the insert.

7_7 Attenuation of thermal, epithermal fluxes and threshold reaction rates in an iron-water mixture.

8_7 a) Scheme of the core
    b) Scheme of the Geometry used for QAD
    c) Scheme of the Geometry used for SABINE.

9_7 Power distribution used for QAD.

TABLE I

Al (n, α) reaction rates $(s^{-1} g^{-1})$

Reactor loading

271-I; 3 Mw			279-I; 7 Mw		
z (cm)	R.R. $(s^{-1} g^{-1})$	ε^* %	z (cm)	R.R. $(s^{-1} g^{-1})$	ε %
1	8,80/7**		2	2,85/8	
11	2,02/7		8,7	8,68/7	
41	4,17/5		13,7	3,98/7	
81	4,40/3		18,7	1,93/7	
121	7,1 /1	< 5	23,7	9,76/6	
151	4,2 /0	8	28,7	5,04/6	
181	2,3 /-1	60	38,7	1,41/6	
			48,7	4,22/5	
			68,7	4,30/4	
			88,7	4,94/3	
			108,7	6,23/2	< 1
			128,7	8,28/1	1
			148,7	1,23/1	1,5
			168,7	1,91/0	3
			188,9	3,09/-1	7
			208,9	4,71/-2	36

ε^* = Statistical counting error

(**): $n/x = n. \ 10^x$

TABLE - II

Euracos results (thermal flux and reaction rates). Values with * are corrected for streaming; $n/x = n.10^x$.

Dy (n,γ)			Au(n,γ)/Cd			In(n,n^1)			S (n,p)			Al$(n\,a)$		
z (cm)	Th.flux $(cm^{-2}s^{-1})$	ε %	z (cm)	R.R. $(s^{-1}g^{-1})$	ε %	z (cm)	R.R. $(s^{-1}g^{-1})$	ε %	z (cm)	R.R. $(s^{-1}g^{-1})$	ε %	z (cm)	R.R. $(s^{-1}g^{-1})$	ε %
1,0	5,51/9		1,0	3,39/8		1,40	3,68/6		1,30	5,94/6		1,10	5,80/4	
6,0	1,10/10		5,30	2,63/8		5,80	1,45/6		5,6	2,56/6		5,40	3,02/4	
11,0	1,64/9		10,40	1,20/8		10,80	6,07/5		10,7	1,13/6		10,50	1,55/4	
12,50	7,61/8		12,20	9,13/7		12,40	5,40/5		12,5	8,64/5		12,30	1,14/4	
19,50	9,21/7		19,30	3,15/7		19,40	1,74/5		19,6	2,54/5		19,40	3,77/3	
23,50	3,43/7		23,30	1,73/7		23,40	9,79/4		23,6	1,20/5		23,40	2,00/3	
25,50	8,80/7		25,60	1,17/7		25,60	5,86/4		25,9	7,20/4		25,70	1,21/3	
30,50	2,42/8		27,60	1,06/7		28,50	3,16/4		26,4	6,14/4		30,30	7,16/2	
35,50	4,16/7		30,20	6,51/6		31,50	1,71/4		30,4	3,34/4		35,10	4,18/2	
37,50	8,96/6		35,40	2,48/6		35,40	1,19/4		30,5	3,44/4		37,40	2,85/2	
41,50	9,78/5		37,30	1,67/6		37,40	8,37/3		35,1	1,83/4		41,40	1,54/2	
47,15	3,66/5		41,30	8,18/5		41,40	4,76/3		35,2	1,69/4		46,85	6,64/1	
51,75	3,55/5		46,65	3,56/5		46,65	2,07/3		37,6	1,24/4		51,45	5,65/1	
56,35	3,69/5		51,25	3,45/5		51,25	2,02/3	1	41,6	6,34/3		56,05	5,33/1	
59,30	1,03/6		55,85	3,41/5		55,85	1,94/3	3	48,0	2,37/3		59,0	4,07/1	
60,40	2,15/6		59,00	3,39/5		59,0	1,76/3	4	52,6	2,14/3		60,60	3,01/1	
70,90	2,43/6		60,60	2,82/5		65,00	4,57/2	5	57,2	1,99/3		60,75	3,78/1	
82,40	1,57/5		65,85	1,15/5		70,50	1,87/2	8	59,3	1,55/3		61,25	2,86/1	
92,90	8,52/3		71,90	2,33/4		75,50	6,37/1	13	60,8	1,31/3		71,55	8,72/0	
94,90	1,97/3		76,75	7,72/3		80,50	2,85/1	5	72,2	2,32/2		72,0	8,27/0	
98,90	2,77/2		80,20	2,80/3		85,50	1,62/1	5	80,5	7,19/1		75,65	6,92/0	
102,90	2,49/2		86,15	1,15/3					81,10	6,98/1		82,95	2,47/0	1
105,90	1,24/3		92,80	6,40/2					90,2	2,34/1		92,70	9,60/-1	2
110,90	2,88/3		94,70	4,28/2					90,9	2,08/1		94,80	5,26/-1	5
115,90	5,32/2	2	98,70	3,16/2					95,0	1,29/1		103,10	1,25/-1	13
118,90	6,24/1	2	102,7	2,31/2					98,9	6,31/0		106,30	1,00/-1	13
122,90	1,34/1	5	106,0	1,52/2					102,9	3,27/0		108,25	5,32/-2	10
126,90	1,46/1	13	108,5	1,07/2					108,2	1,31/0		115,70	3,05/-2	13
128,90	6,36/1	10	113,45	6,04/1	1				110,7	8,28/-1	2			20
139,80	3,80/1	10	118,60	3,03/1	2				113,7	7,16/-1	3			
139,80	3,40/1 *		122,60	1,33/1	4				129,55	5,46/-2	5			
149,80	1,98/1	12	129,0	6,00/0	11				144,25	1,49/-2	5			
149,80	4,0/0 *		135,0	3,71/0	15				144,25	7,9 /-3 *	5			
			135,0	3,59/0 *					150,40	1,64/-3				
			139,15	1,46/0	35				150,40	4,0 /-4 *	10			
			139,15	1,24/0 *					153,0	2,41/-4	10			
			143,70	1,35/0	37									
			143,70	9,7 /-1*										
			147,65	7,48/-1	60									
			147,65	9,8 /-2*										
			151,40	1,91/0	23									
			152,50	5,74/0	18									

TABLE - III

Values of A_i coefficients used in QAD - $A_3=A_4=0$.

I: $d < 20$ cm - II: 20 cm $< d <$ 120 cm - III: $d > 120$ cm

Energy (MeV)	Range	A_o	A_1	A_2
10	I	-7.0632	-6.7966/-2	-4.7964/-4
	II	-6.9569	-8.2070/-2	-3.0930/-5
	III	-6.5115	-8.9493/-2	0.0
8	I	-5.4968	-7.5141/-2	-3.3783/-4
	II	-5.4023	-8.5463/-2	-4.0707/-5
	III	-4.8161	-9.5233/-2	0.0
6	I	-3.9954	-8.6042/-2	-3.1700/-4
	II	-3.8668	-9.8638/-2	+7.0389/-6
	III	-3.9682	-9.6949/-2	0.0
5	I	-3.2834	-9.0754/-2	-4.2298/-4
	II	-3.1062	-1.0889/-1	+5.2499/-5
	III	-3.8622	-9.6300/-2	0.0
4	I	-2.6064	-8.2429/-2	-1.2208/-3
	II	-2.2293	-1.2748/-1	+1.3977/-4
	III	-4.2420	-9.3935/-2	0.0
3	I	-1.9805	-8.8271/-2	-1.2836/-3
	II	-1.5573	-1.3878/-1	+1.9605/-4
	III	-4.3804	-9.1728/-2	0.0
2	I	-1.4313	-9.4567/-2	-1.2418/-3
	II	-9.8306/-1	-1.4801/-1	+2.4563/-4
	III	-4.5201	-8.9059/-2	0.0
1	I	-1.0584	-7.9836/-2	-1.8744/-3
	II	-5.0610/-1	-1.5372/-1	+2.7869/-4
	III	-4.5192	-8.6834/-2	0.0
0.67	I	-1.0272	-3.9426/-2	-3.4588/-3
	II	-3.5757/-1	-1.5000/-1	+2.5256/-4
	III	-3.994	-8.9286/-2	0.0
0.33	I	-1.1394	+3.2164/-2	-6.2191/-3
	II	-2.3550/-1	-1.4348/-1	+2.0862/-4
	III	-3.2396	-9.3411/-2	0.0

TABLE - IV

Water removal cross sections used for SABINE

Removal group	Upper emergy limit	σ_R (barns)		
		A	B	C
1	18	2,4	2,14	2,14
2	16,5	2,5	2,22	2,22
3	15	2,6	2,31	2,31
4	14	2,7	2,40	2,40
5	13	2,8	2,49	2,49
6	12	2,9	2,52	2,52
7	11	3,0	2,55	2,55
8	10	3,1	2,56	2,56
9	9	3,4	2,83	2,83
10	8	3,4	3,15	3,20
11	7	3,5	3,24	3,24
12	6,06	3,7	3,60	3,60
13	5,2	4,0	3,95	3,95
14	4,4	4,8	5,20	5,30
15	3,68	5,6	6,20	6,30
16	3	5,5	5,50	5,50
17	2,23	7,0	7,30	7,30
18	1,35	9,5	9,80	8,30
19	0,821	10	11,20	10,70

TABLE - V

Activation cross sections averaged over QAD groups

Group	Energy (MeV)	In(n,n') (cm^2 . g^{-1})	S(n,p) (cm^2 . g^{-1})	Al(n,) (cm^2 . g^{-1})
1	12-9	1,18/-3	6,20/-3	2,169/-3
2	9-7	1,49/-3	5,97/-3	9,413/-4
3	7-5,5	1,63/-3	5,49/-3	1,043/-4
4	5,5-4,5	1,66/-3	4,63/-3	--
5	4,5-3,5	1,65/-3	4,48/-3	--
6	3,5-2,5	1,59/-3	1,91/-3	--
7	2,5-1,5	1,51/-3	6,92/-4	--
8	1,5-0,835	1,22/-3	--	--
9	0,835-0,5	6,84/-4	--	--
10	0,5-0,1	--	--	--
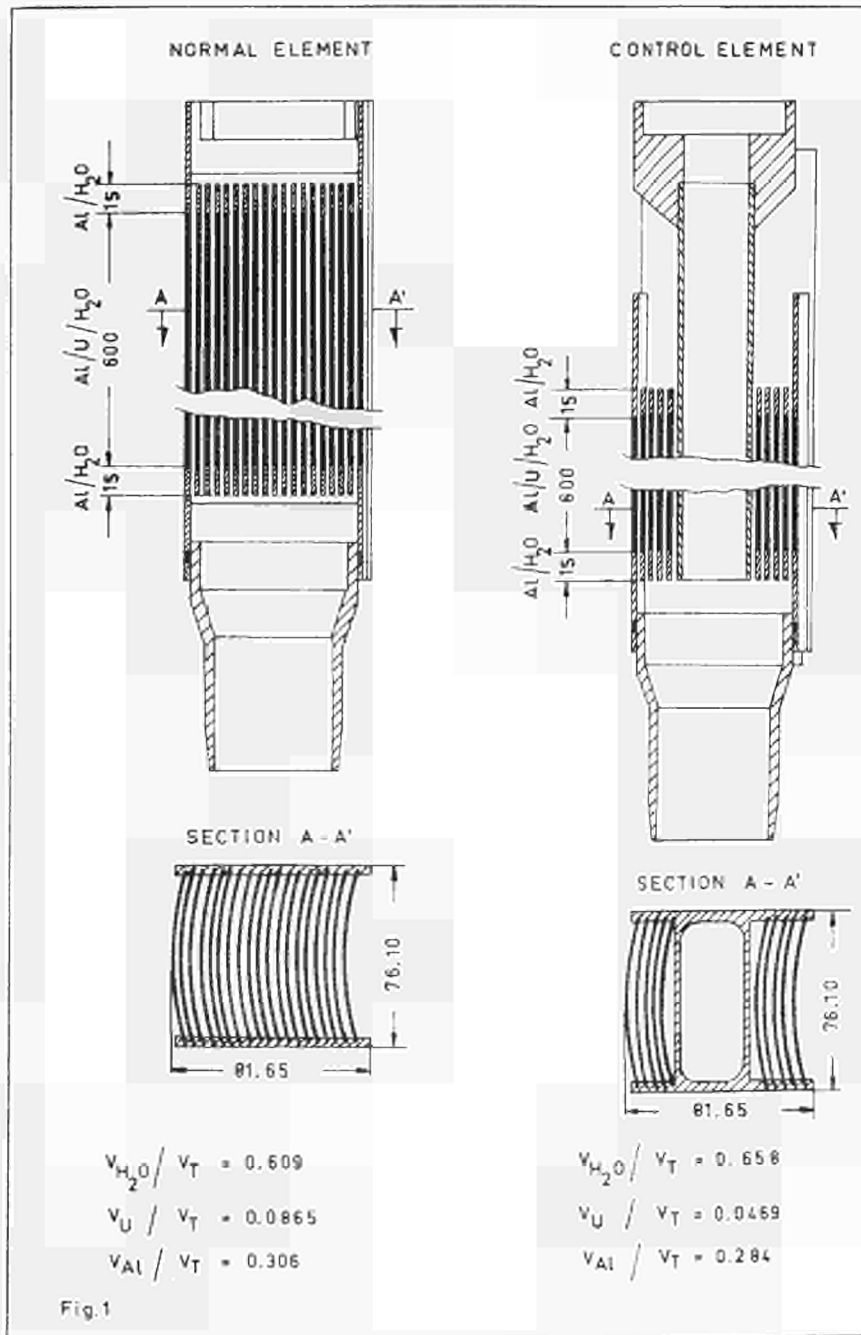
Fig. 1 - Fuel elements (standard and control) of Avogadro RS1 reactor.
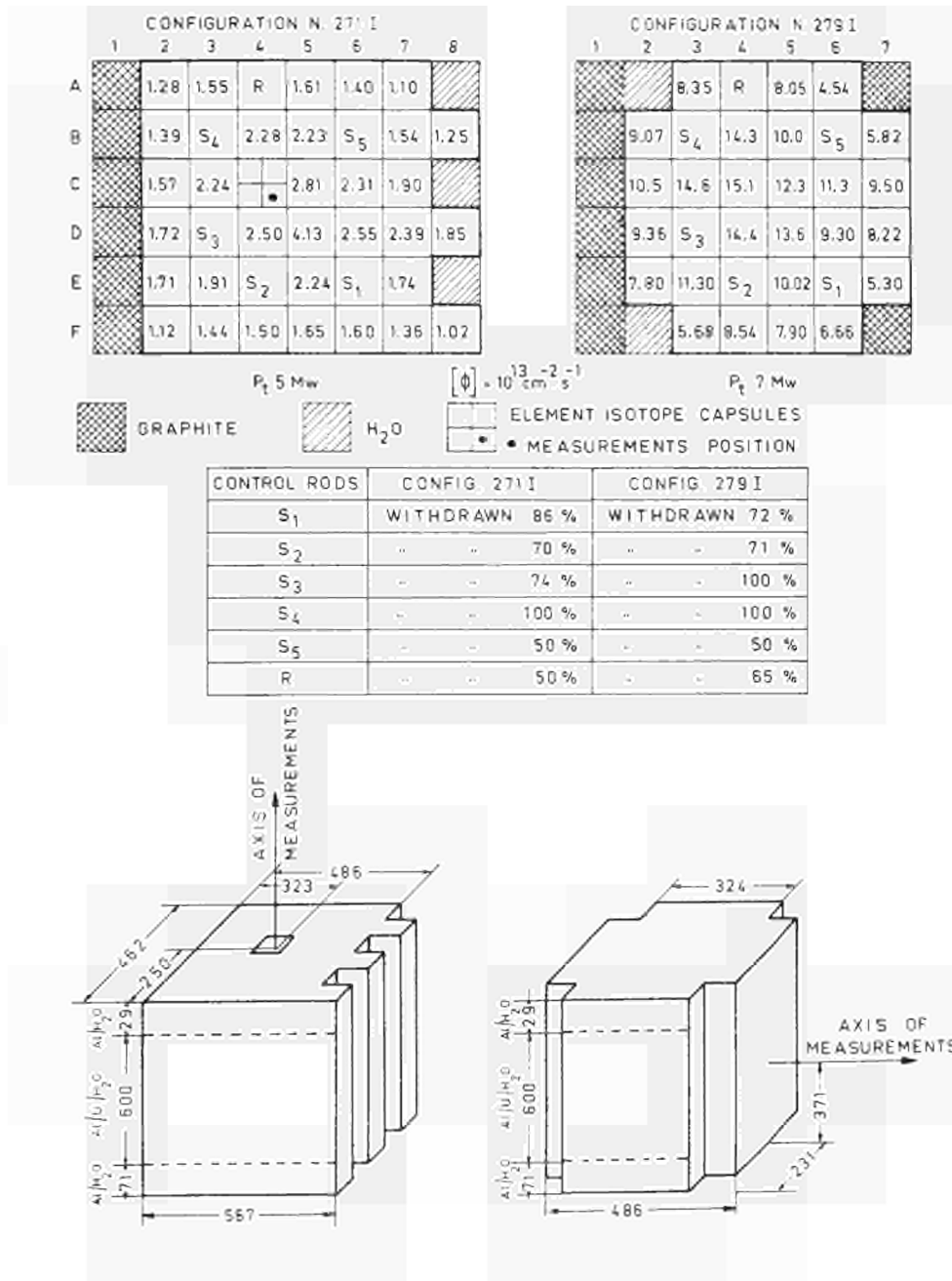
Fig. 2 - Scheme of the reactor loading used for the water
esperiments. Numbers inside elements are proportional
to the thermal flux values.
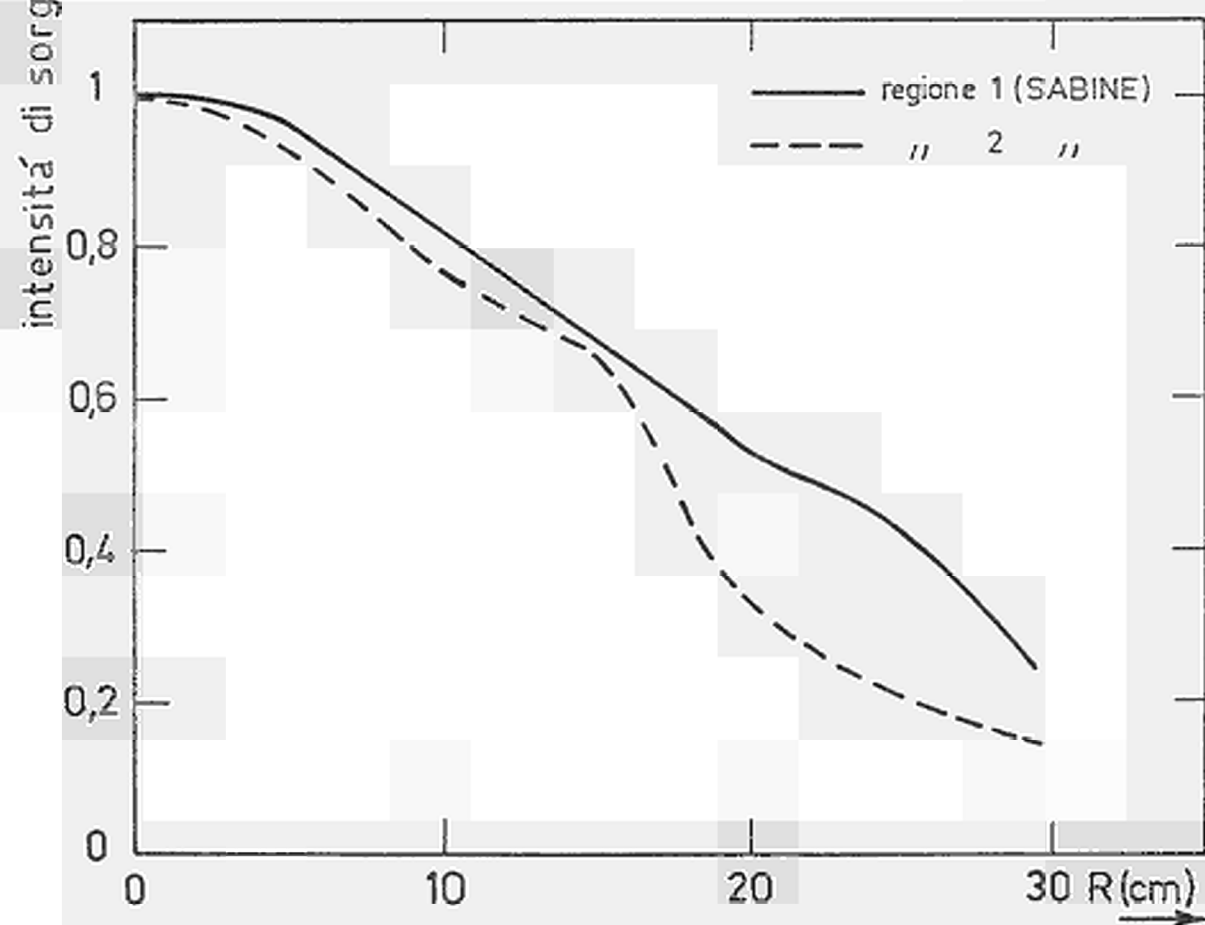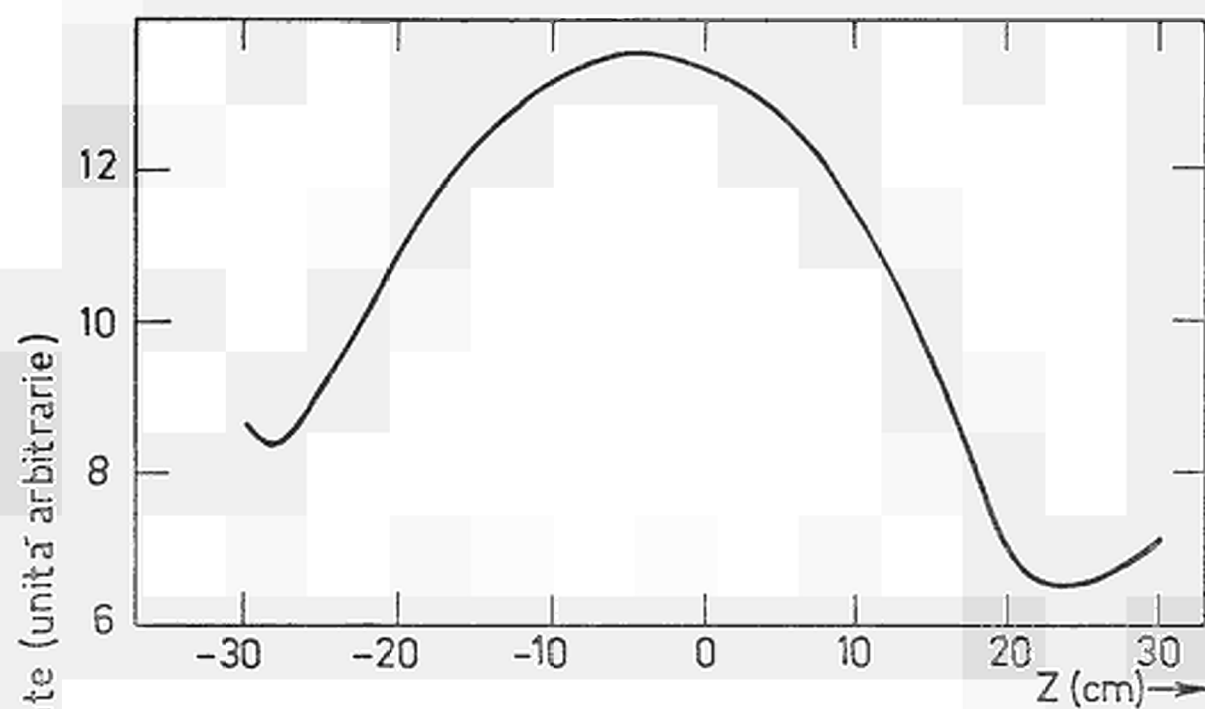
Fig. 3 - Vertical and radial power distribution (average values).
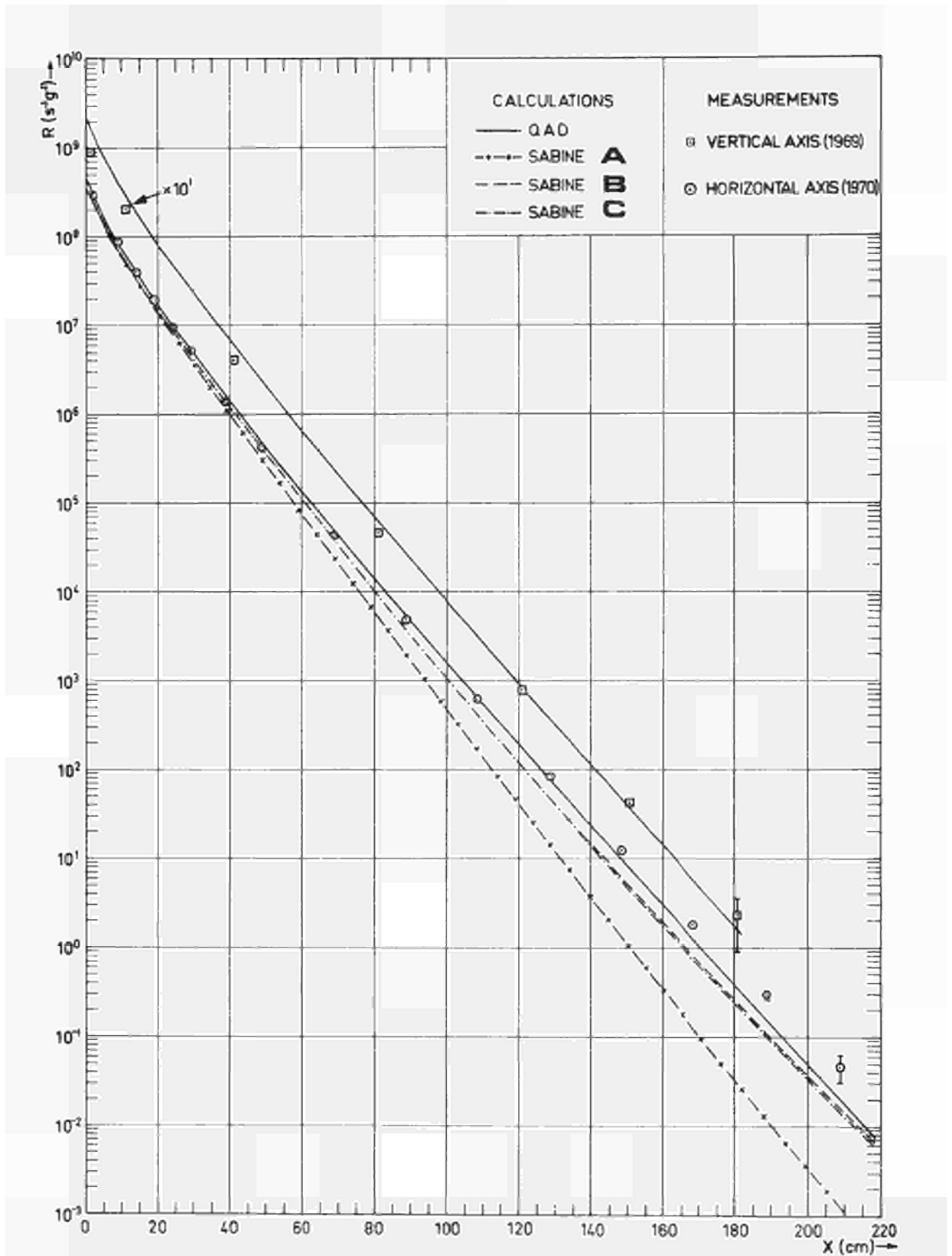
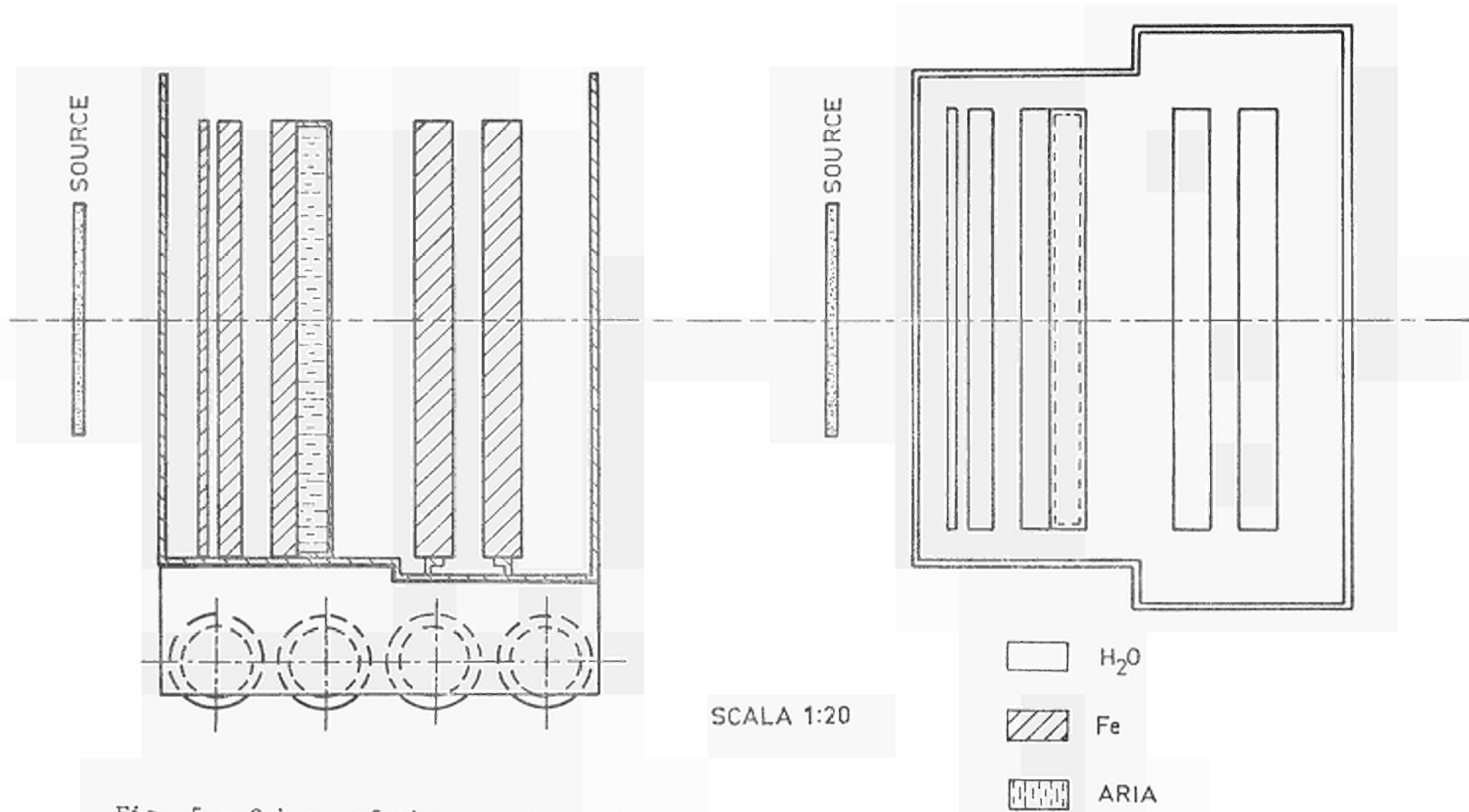Fig. 4 - Attenuation of the Al^{27} (n, α) reaction rate in water.

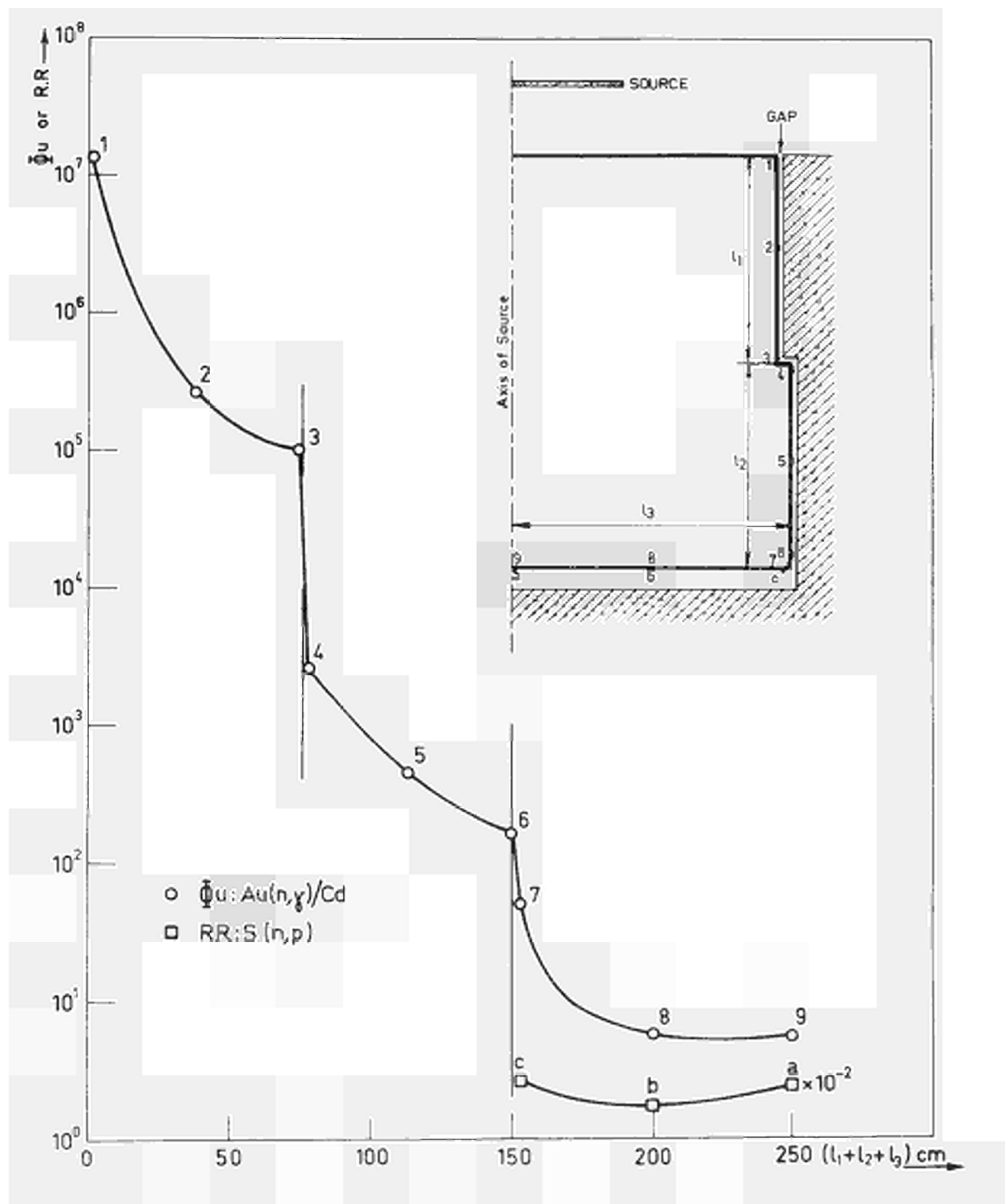Fig. 5 - Scheme of the experimental set-up used for iron-water experiments.

SCALA 1:20

H₂O → H_2O
Fe
ARIA

Fig. 6 - Neutron (fast and epithermal) streaming around the gap shown in the insert.
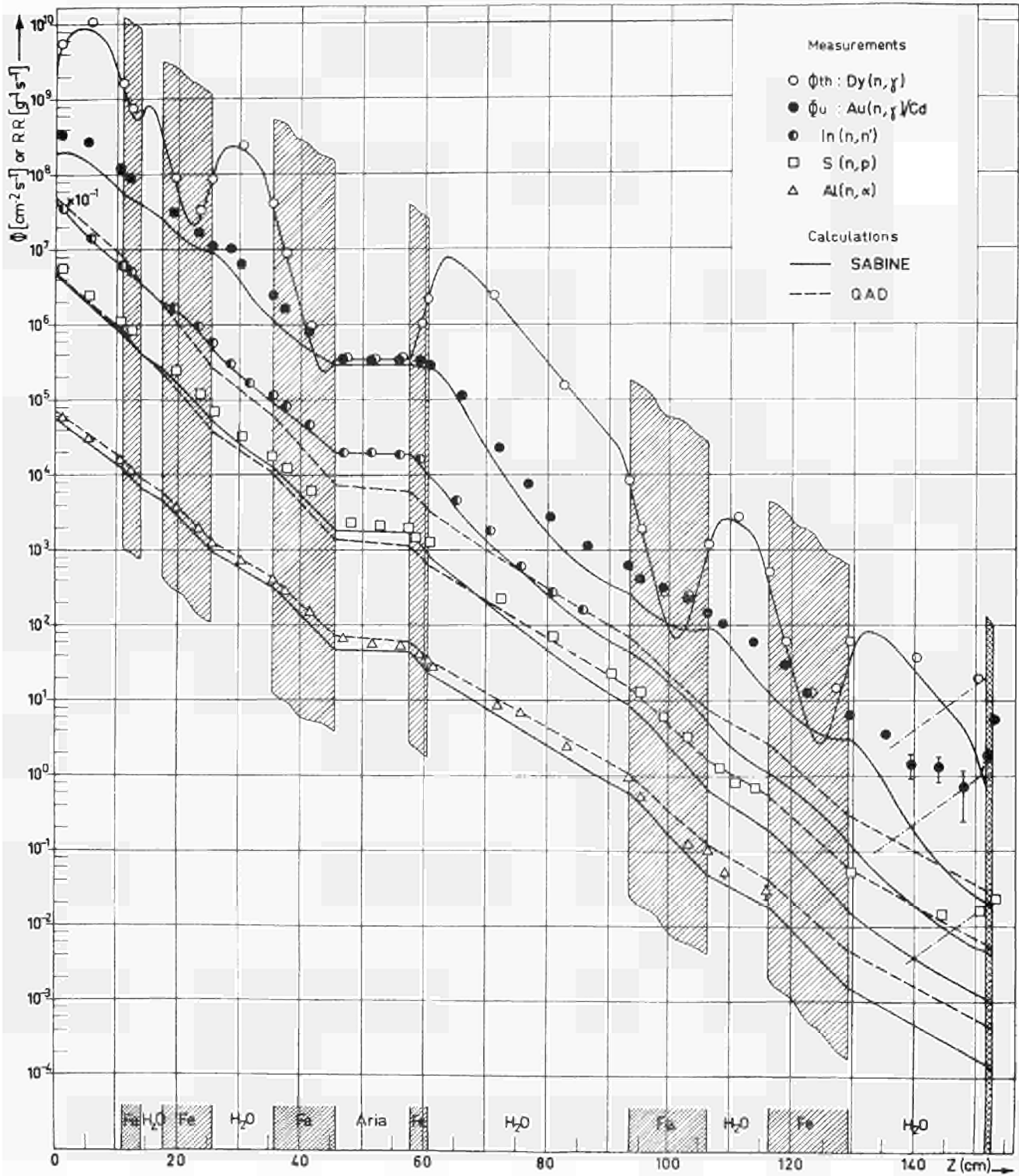
Fig. 7 - Attenuation of thermal, epithermal fluxes and threshold
reaction rates in an iron-water mixture.
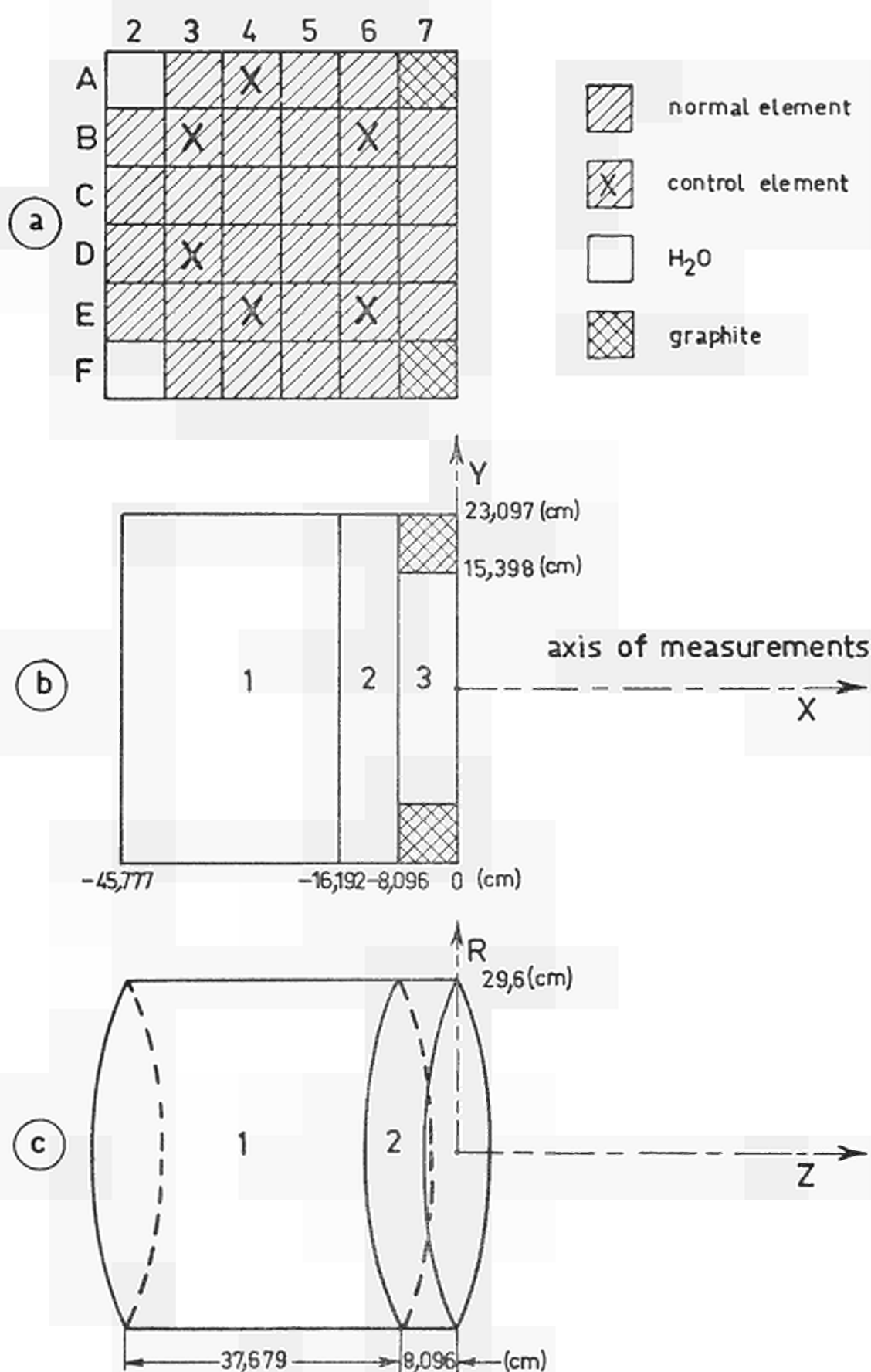
Fig 8 — a) Scheme of the core
b) Scheme of the Geometry used for QAD
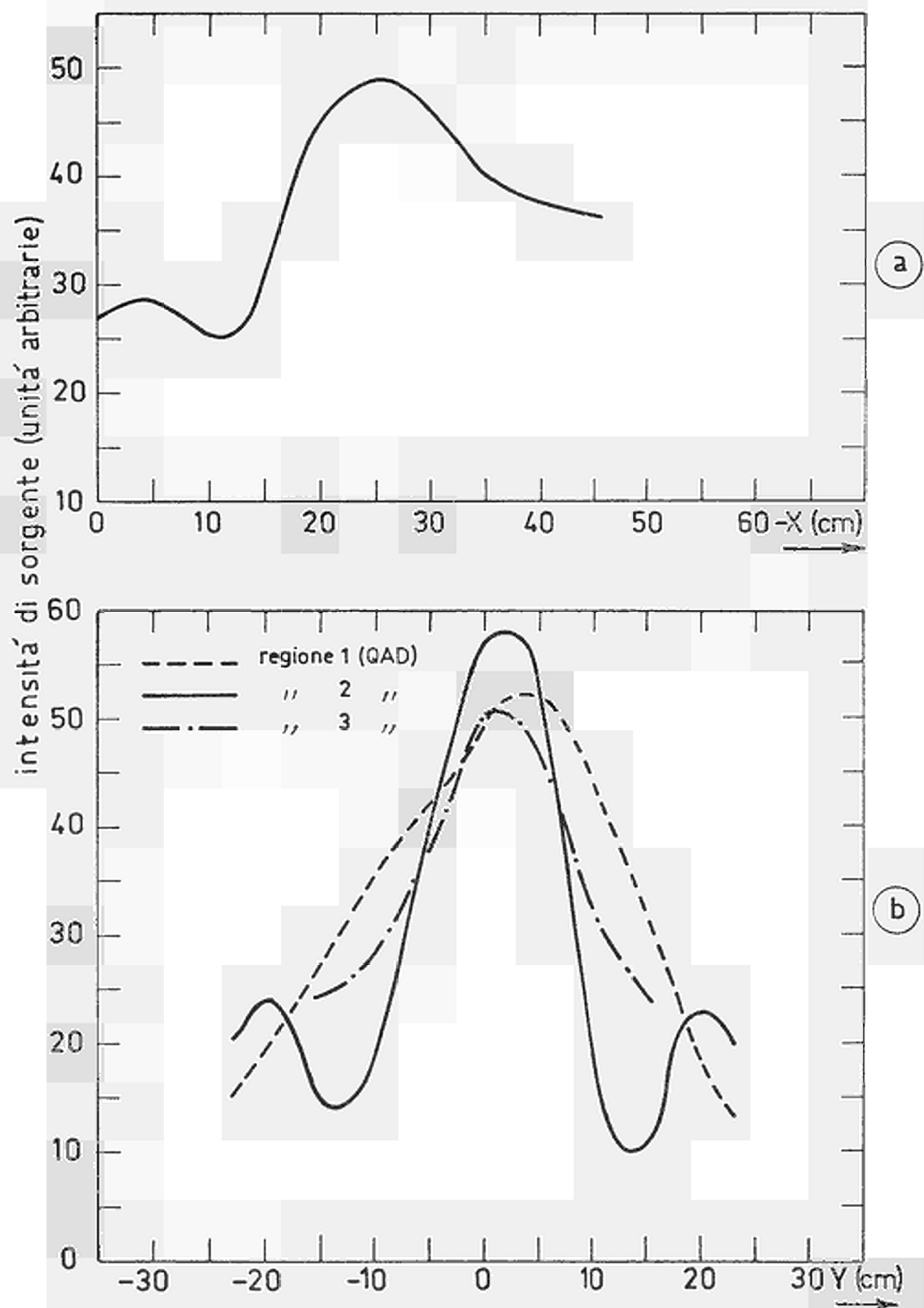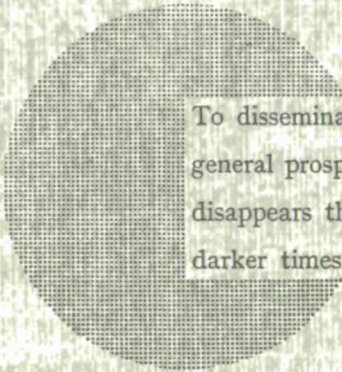c) Scheme of the Geometry used for SABINE.

Fig. 9 - Power distribution used for QAD.

To disseminate knowledge is to disseminate prosperity — I mean general prosperity and not individual riches — and with prosperity disappears the greater part of the evil which is our heritage from darker times.

Alfred Nobel

SALES OFFICES

The Office for Official Publications sells all documents published by the Commission of the European Communities at the addresses listed below, at the price given on cover. When ordering, specify clearly the exact reference and the title of the document.

GREAT BRITAIN AND THE COMMONWEALTH

H.M. Stationery Office
P.O. Box 569
London S.E. 1

UNITED STATES OF AMERICA

European Community Information Service
2100 M Street, N.W.
Suite 707
Washington, D.C. 20 037

BELGIUM

Moniteur belge — Belgisch Staatsblad
Rue de Louvain 40-42 — Leuvenseweg 40-42
1000 Bruxelles — 1000 Brussel — Tel. 12 00 26
CCP 50-80 — Postgiro 50-80

Agency :
Librairie européenne — Europese Boekhandel
Rue de la Loi 244 — Wetstraat 244
1040 Bruxelles — 1040 Brussel

GRAND DUCHY OF LUXEMBOURG

*Office for official publications
of the European Communities*
Case postale 1003 — Luxembourg 1
and 29, rue Aldringen, Library
Tel. 4 79 41 — CCP 191-90
Compte courant bancaire : BIL 8-109/6003/200

FRANCE

*Service de vente en France des publications
des Communautés européennes*
26, rue Desaix
75 Paris-15ᵉ — Tel. (1) 306.5100
CCP Paris 23-96

GERMANY (FR)

Verlag Bundesanzeiger
5 Köln 1 — Postfach 108 006
Tel. (0221) 21 03 48
Telex : Anzeiger Bonn 08 882 595
Postscheckkonto 834 00 Köln

ITALY

Libreria dello Stato
Piazza G. Verdi 10
00198 Roma — Tel. (6) 85 09
CCP 1/2640

Agencies :
00187 Roma   — Via del Tritone 61/A e 61/B
00187 Roma   — Via XX Settembre (Palazzo
                   Ministero delle finanze)
20121 Milano — Galleria Vittorio Emanuele 3
80121 Napoli   — Via Chiaia 5
50129 Firenze — Via Cavour 46/R
16121 Genova — Via XII Ottobre 172
40125 Bologna — Strada Maggiore 23/A

NETHERLANDS

Staatsdrukkerij- en uitgeverijbedrijf
Christoffel Plantijnstraat
's-Gravenhage — Tel. (070) 81 45 11
Giro 425 300

IRELAND

Stationery Office
Beggar's Bush
Dublin 4

SWITZERLAND

Librairie Payot
6, rue Grenus
1211 Genève
CCP 12-236 Genève

SWEDEN

Librairie C.E. Fritze
2, Fredsgatan
Stockholm 16
Post Giro 193, Bank Giro 73/4015

SPAIN

Libreria Mundi-Prensa
Castello, 37
Madrid 1

OTHER COUNTRIES

*Sales Office for official publications
of the European Communities*
Case postale 1003 — Luxembourg 1
Tel. 4 79 41 — CCP 191-90
Compte courant bancaire : BIL 8-109/6003/200